Journal of Molecular Modeling (2020) 26: 105
https://doi.org/10.1007/s00894-020-04354-z

ORIGINAL PAPER

A density functional theory exploration on the Zn catalyst for acetylene hydration

Junqing Li[1,2] · Yu Zhao[1] · Mingyuan Zhu[1,2] · Lihua Kang[1,2]

Received: 12 September 2019 / Accepted: 16 March 2020 / Published online: 19 April 2020

Abstract

The acetylene hydration method to produce acetaldehyde has been widely used for over 130 years; however, a detailed molecular-level understanding of the reaction mechanism is still lacking. In the present work, we systematically investigated the mechanisms of such reactions on $ZnCl_2$, Zn(OH) Cl, and $Zn(OH)_2$ catalysts through density functional theory (DFT) methods. The Fukui function, condensed Fukui function, and Hirshfeld charges enabled us to predict the active sites of the catalysts and acquire electron transfer information. From these data, we found that catalysts bearing hydroxyl groups exhibited relatively low adsorption performances compared with catalysts without this functionality. The calculations demonstrated that the three studied catalysts had three distinct reaction paths. For the Zn(OH)Cl and $Zn(OH)_2$ catalysts, the reaction took place through a one-shift H_2O molecule transfer route, avoiding higher energy barrier pathways. Interestingly, we found that the energy required for breaking the O–H bond in water determined the activation energy of the studied catalytic reactions. The activation barrier increased in the order $Zn(OH)Cl \approx Zn(OH)_2 < ZnCl_2$. This trend suggests that Zn(OH)Cl and $Zn(OH)_2$ are promising catalysts for the hydration of acetylene.

Keywords DFT · Acetylene hydration · Zn catalysts

Introduction

Acetylene (C_2H_2) is an important raw material for the coal chemical industry in China. The naturally occurring fossil fuel can be obtained from abundant coal reserves, especially in the western region. With the rise of petroleum prices and the increase in demand for chemical industry sites, developing sustainable acetylene production methods is an important focus of researchers [1–5]. Furthermore, acetylene is an important hydrocarbon source for large-scale preparations of oxygenated products, such as acetone, acetic acid, and acetaldehyde [6–8]. Among them, acetaldehyde is an important organic chemical intermediate, which can be used in the production of acetic acid, acetate, pentaerythritol, crotonaldehyde, trichloroacetaldehyde, glyoxal, vinyl acetate, and pyridine compounds and has a wide range of applications in pesticides, medicine, food, and feed additives. As such, there is a great demand for acetaldehyde in industry, exceeding a global production of 10^6 tons per year [9–13].

Since 1916, industrial acetylene has been utilized in the production of its hydration products, indicating the importance of acetylene as a chemical raw material [7]. The two main routes for producing acetaldehyde are the direct oxidation of ethylene and the hydration of acetylene. In many developed countries, the direct oxidation of ethylene to acetaldehyde is an attractive approach. However, water is widely used in organic synthesis owing to its low price and nontoxicity [14, 15], and green, environmentally benign processes that maximize economic benefits are among the goals of chemical technology. Thus, the hydration of acetylene has received increased attention as the preferred route for the production of acetaldehyde in China and other countries that would benefit from abundant coal resources [7, 16].

The hydration of acetylene was first reported in 1881 by Kutscheroff [17]. Since this seminal work, many researchers

Electronic supplementary material The online version of this article (https://doi.org/10.1007/s00894-020-04354-z) contains supplementary material, which is available to authorized users.

✉ Lihua Kang
kanglihua@shzu.edu.cn

[1] School of Chemistry and Chemical Engineering of Shihezi University, Shihezi 832000, Xinjiang, China

[2] Key Laboratory for Green Processing of Chemical Engineering of Xinjiang Bingtuan, Shihezi 832000, Xinjiang, China

have investigated the use of transition metals as active catalysts in acetylene hydration reactions (e.g., Cu^{2+}, Cd^{2+}, Hg^{2+}, Ag^{+}, Ru^{2+}, and Zn^{2+}) [18–21]. In these studies, cationic sites have been shown to be more active for acetylene hydrations than negatively charged species. In another study, Dai et al. [22] investigated the reactivity of a Cu(I)–S catalyst with DFT calculations; however, these calculations were limited to the relative energy of the intermediates. Other works have shown that Hg^{2+}, Cu^{2+}, and Ag^{+} are more likely to be reduced to the respective zero-valent metals by acetylene, causing a reduction in the catalyst's activity. In addition, the high toxicity and volatility of cadmium make it harmful for both industrial workers and the entire ecosystem [23]. Therefore, considering reactivity and economic and environmental factors, active zinc has shown promise as a suitable, active component to replace cadmium in acetylene hydration processes. Wang et al. [24–26] demonstrated the use of zinc chloride ($ZnCl_2$) as a catalyst for acetylene hydration, which displayed high catalytic activity (96.1% C_2H_2 conversion). The researchers characterized the surface acid sites of the catalysts and proposed that $Zn(OH)^{+}$ may serve as an active compound in the transformation via XPS analysis. Despite these experimental findings, the authors did not theoretically investigate the reaction mechanism at the molecular level, limiting our full understanding of the reaction.

In the present work, we elucidate the reaction mechanisms of Zn catalysts in acetylene hydration reactions via computational approaches. It is worth noting that theoretical studies on acetylene hydration are rare. Cooksy et al. [27] presented a computational model based on DFT calculations for the hydration of acetylene to form acetaldehyde on the organotransition metal fragment $CpRu(PMe2Im')_2^{+}$ (where Me = methyl and Im ′ = 1,4-dimethylimidazol-2-yl). The researchers predicted a ten-step reaction mechanism, and the results showed that the highest predicted activation barrier was 28.4 kcal mol^{-1}. In another report, Najafian et al. employed computational techniques to study acetylene hydration by six bioinspired catalytic models [28]. Despite these advances, atomistic-level insights on processes occurring at the surface of Zn catalysts remain scarce. As such, we sought to design and investigate acetylene hydration reactions over Zn-based catalysts, i.e., $ZnCl_2$, a new catalyst Zn(OH)Cl, and $Zn(OH)_2$. We anticipate that a new understanding on the mechanism of Zn-catalyzed acetylene hydrations would help to inform the design of promising industrial catalysts.

Computational methods

All DFT calculations were carried out via the Gaussian 09 software package [29]. Geometric optimizations of the co-adsorption species, intermediates (Ims), transition states (Ts), and de-adsorption species were calculated with the B3LYP hybrid functional, which combined Becke's three-parameter exchange functional (B3) and the Lee–Yang–Parr (LYP) functional in conjunction with the Los Alamos effective core pseudo-potential basis set LANL2DZ for zinc atoms, and the 6-31++G** basis set for carbon, hydrogen, oxygen, and chlorine atoms [30–34]. The relative energies of all optimized structures along the reaction pathways were zero-point energy corrections at the same level of optimization. We optimized single-adsorption and co-adsorption structures with correction for basis set superposition error (BSSE) [35]. No symmetry constraints were imposed on the geometry optimizations. For the Hessian matrix calculation, all of the stationary points were characterized as minima (no imaginary frequency) or transition states (one imaginary frequency). Intrinsic reaction coordinate (IRC) [36–39] calculations were performed to confirm that the correct products were linked to the corresponding reactants. Transition states were characterized using frequency calculations implemented at the same level of theory by analyzing the vibrational modes.

Fukui function [40] is a very important concept in the conceptual density functional theory, we calculate and visualize it in prediction of reactive sites and adsorption sites in this work. The condensed Fukui function [41] was calculated to analyze the nucleophilicity and electrophilicity of Zn atom. After the condensed Fukui function analysis, we predicted the electron acceptor and donor in the reactions. In order to confirm the reliability of the Fukui function analysis, Hirshfeld population data [42] were cited to analyze electron transfer behavior between the adsorbates and substrates. Adsorption energy (E_{ads}) and co-adsorption energy ($E_{co\text{-}ads}$) calculations were carried out to reveal the adsorption behavior of the catalysts and are defined as follows:

$$E_{ads} = E_{C_2H_2/H_2O+catalyst} - E_{C_2H_2/H_2O} - E_{catalyst} \quad (1)$$

$$E_{co-ads} = E_{C_2H_2+H_2O+catalyst} - E_{C_2H_2} - E_{H_2O} - E_{catalyst} \quad (2)$$

The $E_{C2H2/H2O+catalyst}$ is the whole energy of the system that H_2O or C_2H_2 is adsorbed on the catalyst. The $E_{C2H2+H2O+catalyst}$ is the total system adsorption energy that both of the reactants are adsorbed on the catalyst. Furthermore, E_{C2H2}, E_{H2O}, $E_{catalyst}$ are the energy of the isolated catalyst and the reactants, respectively. The Multiwfn 3.7 program [43] was used to calculate all the Fukui function, condensed Fukui function, and Hirshfeld charges. All reactions were carried out in the gas phase. Fukui function and condensed Fukui function were also calculated in the gas phase, ignoring the effect of solvents [44]. In this work, we chose the Hirshfeld's stockholder approach [45] to calculate condensed Fukui function.

Results and discussion

Geometries for reactants

Reactants used for these calculations included an isolated C_2H_2 molecule, an H_2O molecule, a $ZnCl_2$ molecule, a Zn(OH)Cl molecule, and a $Zn(OH)_2$ molecule. The most stable optimized geometries for the reactants are shown in Fig. 1.

Adsorption of C_2H_2 and H_2O onto catalysts

Figure 2 shows the calculated $f^+$and f^- of the Fukui function for the $ZnCl_2$, Zn(OH)Cl, and $Zn(OH)_2$ catalysts. The $f^+$and f^- of Fukui function for these catalysts were employed to predict their adsorption sites and reactive sites. Table 1 shows the condensed Fukui functions for $ZnCl_2$, Zn(OH)Cl, and $Zn(OH)_2$, as well as the Hirshfeld charges for all atoms of Zn catalysts. With the addition of hydroxyl groups, the positive charge of Hirshfeld charges of Zn atoms increases, indicating that the electrophilicity of Zn atoms is enhanced. The condensed Fukui function f_A^+ of Zn catalysts were bigger than those of f_A^-, indicating that the Zn atom was the acceptor of the electron and it was easy to obtain the electron, which was a nucleophilic attack site. Likewise, the value of f_A^+ and f_A^- of the O atom in Zn(OH)Cl and $Zn(OH)_2$ molecule indicated that O atom was an electrophilic attack site. The presented data show that the f_A^+ of $ZnCl_2$ (0.5217) was smaller than Zn(OH)Cl (0.5286) and $Zn(OH)_2$ (0.5540), suggesting that the hydroxyl group enhanced the chemical reactivity of the Zn catalyst.

The Hirshfeld charges of Zn catalysts and Zn atom for the C_2H_2/H_2O–Zn catalysts adsorption complexes in Table 2 illustrated that electrons could be transferred from the reactant to the Zn catalyst. It further confirmed the veracity of the condensed Fukui function. We also calculated the electrostatic potential (ESP) of Zn catalysts (Fig. S1), showing that the charge population of the Zn catalysts consistent with the conclusion of condensed Fukui function.

In order to find the best adsorption configurations for the reactions, we constructed all possible C_2H_2 and H_2O adsorption sites on the $ZnCl_2$, Zn(OH)Cl, and $Zn(OH)_2$ species manually. The most stable catalyst–C_2H_2 and catalyst–H_2O complexes as well as their configurations are depicted in Fig. 3.

The adsorption energy values of C_2H_2 and H_2O show a lower barrier for the adsorption of H_2O than C_2H_2 on the Zn catalyst surface (Table 3). These data indicate that H_2O is preferentially adsorbed onto the Zn catalysts over C_2H_2. We provided the ESP of single-adsorption of C_2H_2/H_2O–Zn catalysts in the Fig. S2, in order to find the best optimal co-adsorption (co-ads) configuration. ESP analyses of the catalyst–H_2O complexes were carried out to investigate the interactions between C_2H_2 and the adsorption complexes, making it possible to obtain the co-adsorption configurations of the catalysts with H_2O and C_2H_2. In Fig. S3, the ESP of the co-adsorption of reactants and Zn catalysts showed that the color of Zn atom was lighter than in single adsorption; in other words, Zn atom accepted electron from the reactants, The Hirshfeld charges of co-adsorption configuration in Table 4 further confirmed the veracity of the ESP. The co-adsorption energies were shown in Table 4. The $E_{co\text{-}ads}$ of $ZnCl_2$–H_2O–C_2H_2 was − 16.93 kcal/mol. The $E_{co\text{-}ads}$ of the first and the second reaction pathway of Zn(OH)Cl–H_2O–C_2H_2 were − 16.00 kcal/mol and − 18.86 kcal/mol, respectively. Likewise, the $E_{co\text{-}ads}$ of $Zn(OH)_2$ were − 14.77 kcal/mol and − 17.02 kcal/mol.

Reaction mechanisms of acetylene hydration on catalysts

$ZnCl_2$

All possible reaction pathways were systematically investigated to better understand the catalytic mechanism of acetylene hydration. The hydration of acetylene using $ZnCl_2$ as the catalyst proceeded via a concerted reaction mechanism. Figure 4 illustrates the reaction pathways of $ZnCl_2$, which originate from C_2H_2 and $ZnCl_2$–H_2O co-adsorption structures. All geometries of the various stationary points located on the potential energy surface are depicted in Fig. 5.

The most stable adsorption states of the catalyst during activation of the reactants were determined. During the

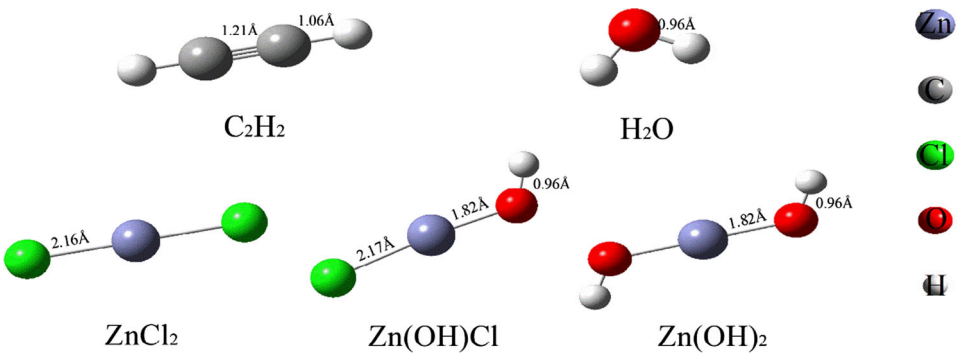

Fig. 1 Optimized structures of C_2H_2, H_2O, $ZnCl_2$, Zn(OH)Cl, and $Zn(OH)_2$. Distances are in Å and angles in degrees. Carbon, hydrogen, chlorine, oxygen, and zinc atoms are depicted in gray, white, green, red, and blue, respectively

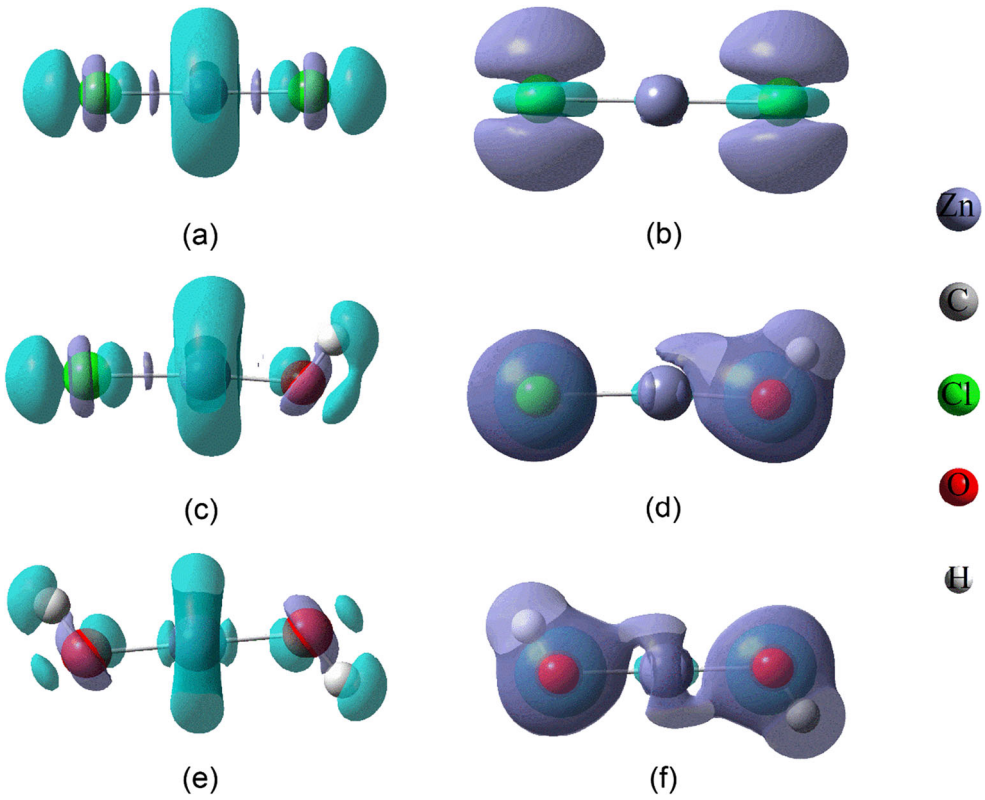

Fig. 2 The calculated Fukui function of $ZnCl_2$ (a(f_A^+), b(f_A^-)), Zn(OH)Cl (c(f_A^+), d(f_A^-)), and $Zn(OH)_2$ (e(f_A^+), f(f_A^-)) (isovalue = 0.002)

formation of the co-adsorption structure with the $ZnCl_2$–H_2O complexes, the bond length of H_2O was largely unchanged, indicating that the H_2O molecule was not activated in the co-adsorption structure. The co-adsorption structure was then transformed into Ims1 via Ts1. At Ts1, the H_4–O bond broke, and its bond length increased from 0.97 to 1.52 Å. Simultaneously, the H_4 atom approached the C=C bond, and the C_1–H_4 distance decreased from 2.35 to 1.22 Å. The distance between the O atom and C_2 atom decreased from 3.11 to 2.24 Å during this transformation. In the transition state structures, the H_4–O bond of H_2O was substantially lengthened, leading to direct H_2O elimination, which indicated the complete activation of H_2O. Our calculations also revealed distortion in the configuration of acetylene in which the angle of H_1–C_1–C_2 decreased from 177.28° to 143.62°. This distortion suggests that there are interactions between C_2H_2 and the H_4 atom.

The only imaginary frequency (− 1302.96 cm^{-1}) was obtained from the vibrational analysis of Ts1, indicating that it is a valid transition state. This frequency was associated with the stretching movement of the H_4 atom. Since the energy barrier of Ts1 was calculated to be 42.78 kcal mol^{-1}, this transformation was assigned as the rate-determining step.

To ensure that this transition state connected the appropriate reactant and product, IRC calculations were performed and confirmed that Ts1 connects the co-adsorption structure and

Table 1 The Hirshfeld charges, condensed Fukui functions for the Zn catalysts

	Atom	q(N)	f_A^-	f_A^+
$ZnCl_2$	Zn	0.5830	0.1863	0.5217
	Cl	− 0.2914	0.4069	0.2389
	Cl	− 0.2914	0.4069	0.2389
Zn(OH)Cl	Zn	0.6035	0.2235	0.5286
	O	− 0.4225	0.3013	0.0825
	H	0.1243	0.0985	0.1871
	Cl	− 0.3051	0.3767	0.1988
$Zn(OH)_2$	Zn	0.6214	0.2661	0.5540
	O	− 0.4303	0.2728	0.0703
	H	0.1196	0.0942	0.1512
	O	− 0.4303	0.2728	0.0703
	H	0.1196	0.0942	0.1512

Table 2 The Hirshfeld charges of Zn catalysts for the C_2H_2/H_2O–Zn catalysts adsorption complexes

Adsorption species	Zn catalysts total charges	Zn atom charges
$ZnCl_2$–C_2H_2	− 0.1634	0.5017
Zn(OH)Cl–C_2H_2	− 0.1502	0.5136
$Zn(OH)_2$–C_2H_2	− 0.1415	0.5223
$ZnCl_2$–H_2O	− 0.2076	0.4928
Zn(OH)Cl–H_2O	− 0.1518	0.5171
$Zn(OH)_2$–H_2O	− 0.1407	0.5269

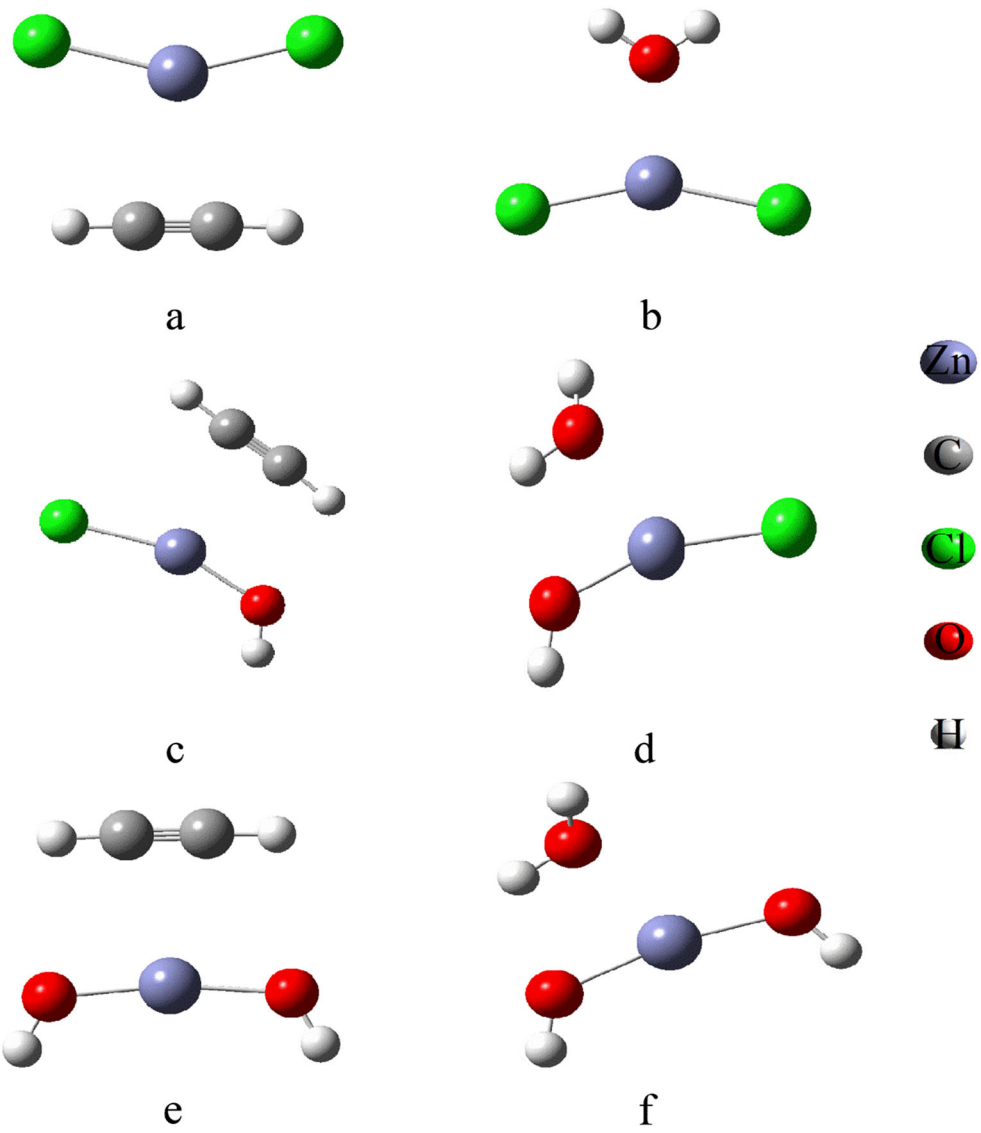

Fig. 3 **a**–**f** the most stable adsorption configurations for C_2H_2/H_2O on the following Zn catalysts: **a** C_2H_2–$ZnCl_2$, **b** H_2O–$ZnCl_2$, **c** C_2H_2–Zn(OH)Cl, **d** H_2O–Zn(OH)Cl, **e** C_2H_2–$Zn(OH)_2$, **f** H_2O–$Zn(OH)_2$

Ims1. At Ims1, the C_1 atom was bonded to the H_4 atom, and the length of C_1–H_4 was shortened to 1.087 Å, which was almost equal to the C_1–H_4 bond length (1.097 Å) of the isolated acetaldehyde molecule. In addition, the O atom is bonded to the C_2 atom in this state with a bond length of 1.39 Å. It is worth noting that this bond length is shorter compared with Ts1. During the final step, the organic product acetaldehyde was produced via tautomerization of vinyl alcohol, which was calculated to be an exothermic process.

Table 3 Optimal adsorption energies (kcal mol^{-1}) of C_2H_2 and H_2O adsorbed separately and co-adsorbed on the catalyst

	$ZnCl_2$	Zn(OH)Cl	$Zn(OH)_2$
H_2O	− 13.94	− 13.48	− 11.80
C_2H_2	− 5.12	− 5.74	− 5.48
co-ads	− 16.93	− 16.00 (1st) − 18.86 (2nd)	− 14.77 (1st) − 17.02 (2nd)

Zn(OH)Cl

The acetylene hydration reaction pathway catalyzed by Zn(OH)Cl was then studied through DFT computations. We found two reaction pathways for the hydration reaction using Zn(OH)Cl as the catalyst which was very distinct from $ZnCl_2$. All geometries and their corresponding energy values in the first kind of the reaction pathway are depicted in Figs. 6 and 7. Owing to the stronger adsorption of H_2O compared with C_2H_2, H_2O was initially adsorbed onto Zn(OH)Cl, followed by adsorption of C_2H_2 onto the H_2O–Zn(OH)Cl complex to form the co-adsorbed intermediate. The adsorbed C_2H_2 molecule was nearly identical in length to the O_2–Zn bond in Zn(OH)Cl. The bond lengths of C_1–C_2 and H_4–O_1 were

Table 4 The Hirshfeld charges of Zn atom for co-adsorption configuration

Adsorption species	Zn catalysts total charges	Zn atom charges
$ZnCl_2$–C_2H_2–H_2O	− 0.3258	0.4334
Zn(OH)Cl–C_2H_2–H_2O–1st	− 0.2161	0.4708
$Zn(OH)_2$–C_2H_2–H_2O–1st	− 0.1783	0.4863
Zn(OH)Cl–C_2H_2–H_2O–2nd	− 0.1379	0.5103
$Zn(OH)_2$–C_2H_2–H_2O–2nd	− 0.1269	0.5157

identical within 0.05 Å, indicating that molecular H_2O was not activated in this state. During the first step, a barrier of 11.26 kcal mol^{-1} was initially overcome, and the co-adsorption structure was transformed into the intermediate state (Ims1) via transition state, Ts1. At Ts1, the Zn(OH)Cl molecule was distorted, with a decrease in the Cl–Zn–O_2 angle from 153.50° to 141.91°. Simultaneously, distortion of C_2H_2 was detected, and the C_1=C_2 and O_2–Zn bonds were slightly lengthened. These calculations revealed that there was an interaction between C_2H_2 and Zn(OH)Cl. Specifically, the C_2 and C_1 atoms of C_2H_2 approached the O_2 and Zn atoms of the catalyst, with the C_2–O_2 and C_1–Zn distances decreasing from 3.02 Å to 2.06 Å and 2.74 Å to 2.24 Å, respectively.

It was determined that Ts1 had only one imaginary frequency (− 386.39 cm^{-1}), indicating that it was a valid transition state, and an energy barrier of 11.26 kcal mol^{-1} was predicted. The IRC calculation of this transition state confirmed that Ts1 connects the co-adsorption intermediate to Ims1, suggesting that no additional intermediates were involved in the first reaction step. At Ims1, the Zn–O_2 bond was broken, followed by bonding of the O_2 and Zn atoms to the C_2 and C_1 atoms, respectively, with lengths of 1.40 Å (O_2–C_2) and 2.01 Å (Zn–C_1). The lengths of the bonds in Ims1 were shortened in comparison to Ts1. In this step, the two carbons in C_2H_2 transformed from a triple bond to a double bond.

Ims1 was shown to lead to Ims2 via Ts2. The pathway to Ts2 was calculated to involve the participation of an H_2O molecule. Specifically, the O_1–H_3 bond of H_2O was substantially elongated from 0.98 Å in Ims1 to 1.24 Å in Ts2, indicating the complete activation of H_2O. Then, the H_3 atom dissociated from the O_1 atom and bonded to the adjacent C_1 atom, and the corresponding H_3–C_1 bond length was shortened to 1.40 Å. Simultaneously, the Zn–C_1 bond was broken, and the O_1 atom bonded to the Zn atom. In this scenario, the length of Zn–C_1 was elongated from 2.01 Å to 2.19 Å. At Ts2, the newly generated Zn(OH)Cl catalyst was identified. The length of the Zn–O_1 bond (2.01 Å) was 0.1 Å longer than that of the Zn–O_2 bond (1.91 Å) in the co-adsorption state. Moreover, the angle of O_1–Zn–Cl (140.11°) was 13.39° smaller than that of O_2–Zn–Cl (153.50°) in the co-adsorption state. To improve the efficiency of the reaction, the enolic group was rotated to make it nearly perpendicular to the Zn(OH)Cl catalyst. However, other significant bonds, such as C_1=C_2 and C_2–O_2, were barely changed during this transformation. The only imaginary frequency (− 1335.21 cm^{-1}) was obtained from the vibrational analysis of the Ts2 structure, which is associated with the stretching movement of the H_3 atom. To access Ts2, Ims1 indicated an energy barrier of 21.14 kcal/mol.

IRC calculations were performed again to confirm that Ts2 could convert to Ims2. In Ims2, the newly generated H_2O molecule from Ims1 was determined to serve as an acid by transferring a proton to C_1 of the vinyl anion to form a vinyl alcohol intermediate. The Zn–O_1 bond was shortened to 1.85 Å during this transformation, and the Cl–Zn–O_1 angle was increased from 140.11° in Ts2 to 152.41° in Ims2, indicating that the newly formed Zn(OH)Cl catalyst became more stable in the latter state. It is worth noting that the length of the O_1–H_3 bond increased by 3.14 Å from Ts2 (1.24 Å), and the length of the C_1–H_3 bond decreased from 1.40 to 1.09 Å. When employing Zn(OH)Cl as the catalyst, the energy barriers for the two steps of the reaction were calculated to be 15.46 and 21.14 kcal mol^{-1}, respectively, with the second step being the rate-determining step. The final step of the reaction was tautomerization of the vinyl alcohol to generate acetaldehyde, which was calculated to be an exothermic process.

Then, we found the second reaction pathway of the Zn(OH)Cl catalyst which is distinct from the first one. All geometries and their corresponding energy values in the second kind of the reaction pathway are depicted in Figs. 8 and 9. In contrast to the reaction pathways catalyzed by $ZnCl_2$, H_2O

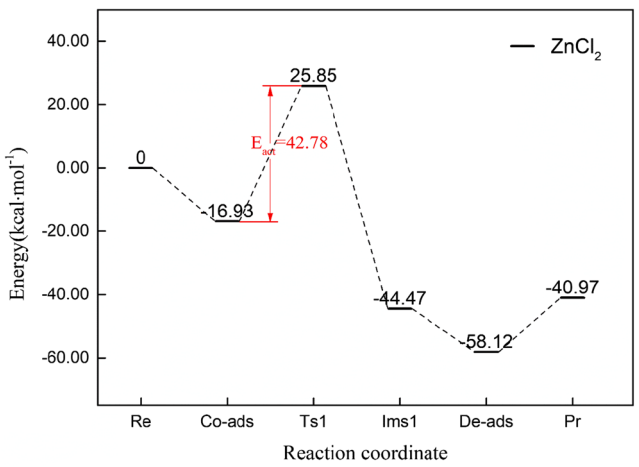

Fig. 4 The energy profiles for the reaction pathway $ZnCl_2$

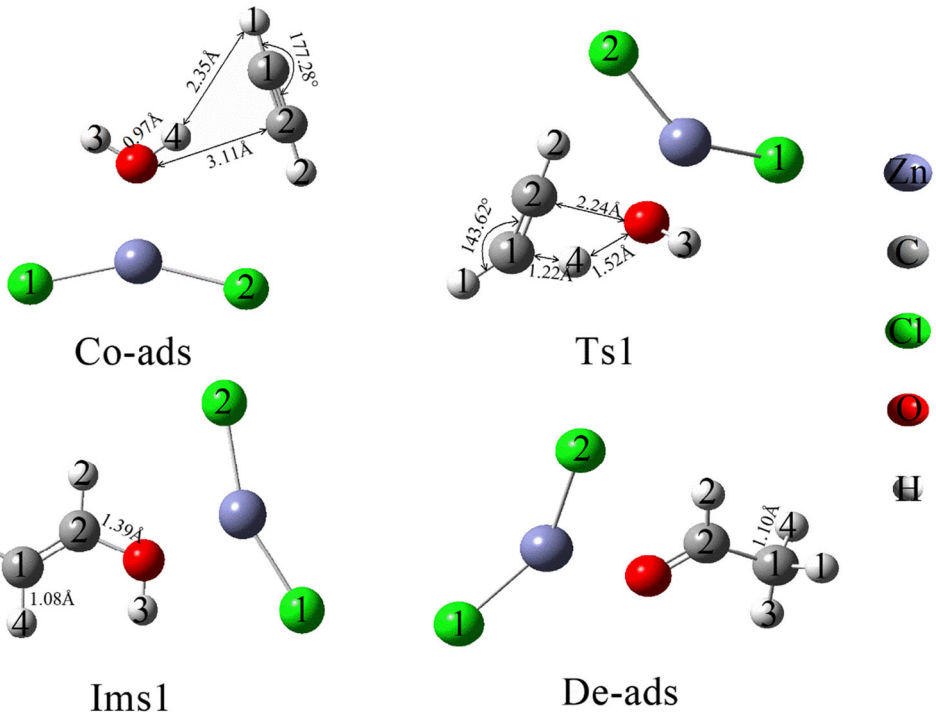

Fig. 5 Optimized structures of stationary points for reaction channel $ZnCl_2$

and the Zn(OH)Cl catalyst both participated in the first step of the reaction. One proton from the H_2O molecule and one hydroxyl group from Zn(OH)Cl were predicted to simultaneously react with the C≡C triple bond of acetylene. In this step, the co-adsorption structure transformed into an intermediate state (Ims1) via a transition state (Ts1). At Ts1, the Zn(OH)Cl molecule was distorted, with a decrease in the O_2–Zn–Cl angle from 155.27° to 124.43°. Simultaneously, distortion of the C_2H_2 molecule was detected, and the O_1–H_3 and O_2–Zn bonds were slightly lengthened. In this state, the O_1–H_3 bond was broken, demonstrating that the H_2O molecule was definitively activated. The H_3 and O_2 atoms approached the C_1 and C_2 atoms, and the C_2–O_2 and C_2–H_3 distances decreased from 2.96 to 1.97 Å and from 2.42 to 1.62 Å, respectively. Identification of distorted acetylene suggested that there were strong interactions between the acetylene molecule, H_3 proton, and Zn(OH)Cl. Only one imaginary frequency was found in Ts1, indicating that it is a valid transition state. The energy barrier for this step was calculated to be 18.11 kcal mol^{-1} relative to the co-adsorption state and was assigned as the rate-determining step.

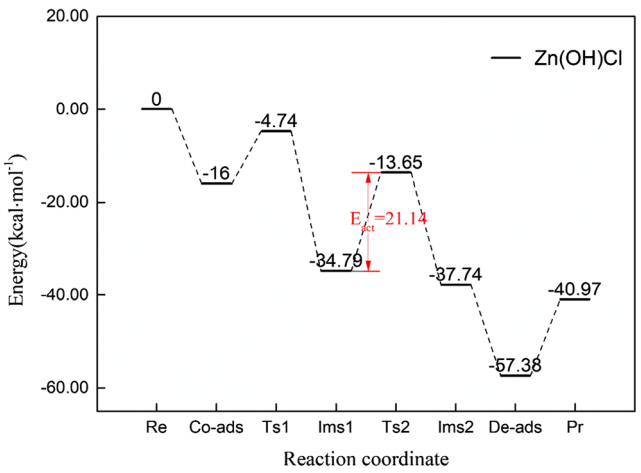

Fig. 6 The energy profiles for the first reaction pathway Zn(OH)Cl

IRC calculations were then carried out and confirmed that Ts1 connected the co-ads state to Ims1. In Ims1, vinyl alcohol was formed, and the Zn(OH)Cl catalyst was regenerated. The O_2–Zn–Cl angle increased from 124.43° to 160.42°, and the C_1 and C_2 atoms were bonded to the separated H_3 and O_2 atoms. The lengths of the C_1–H_3 and C_2–O_2 bonds were 1.40 Å and 1.08 Å, respectively, and both bonds were shortened in comparison to the previous transition state (Ts1).

The final step of this reaction was similar to the previously studied catalysts and involved the release of acetaldehyde following tautomerization of vinyl alcohol. However, in contrast to the previous two catalytic systems, this step was calculated to be an exergonic process for Zn(OH)Cl.

$Zn(OH)_2$

Figures S4, S5, S6, and S7 display two kinds of relevant energy and structures of the acetylene hydration reaction catalyzed by $Zn(OH)_2$. The reaction pathways are similar to the reaction pathways catalyzed by Zn(OH)Cl. We provide only a brief analysis of the two reaction pathways below.

In the first kind of reaction pathway, the reaction converted into three steps. During the first step, a barrier of

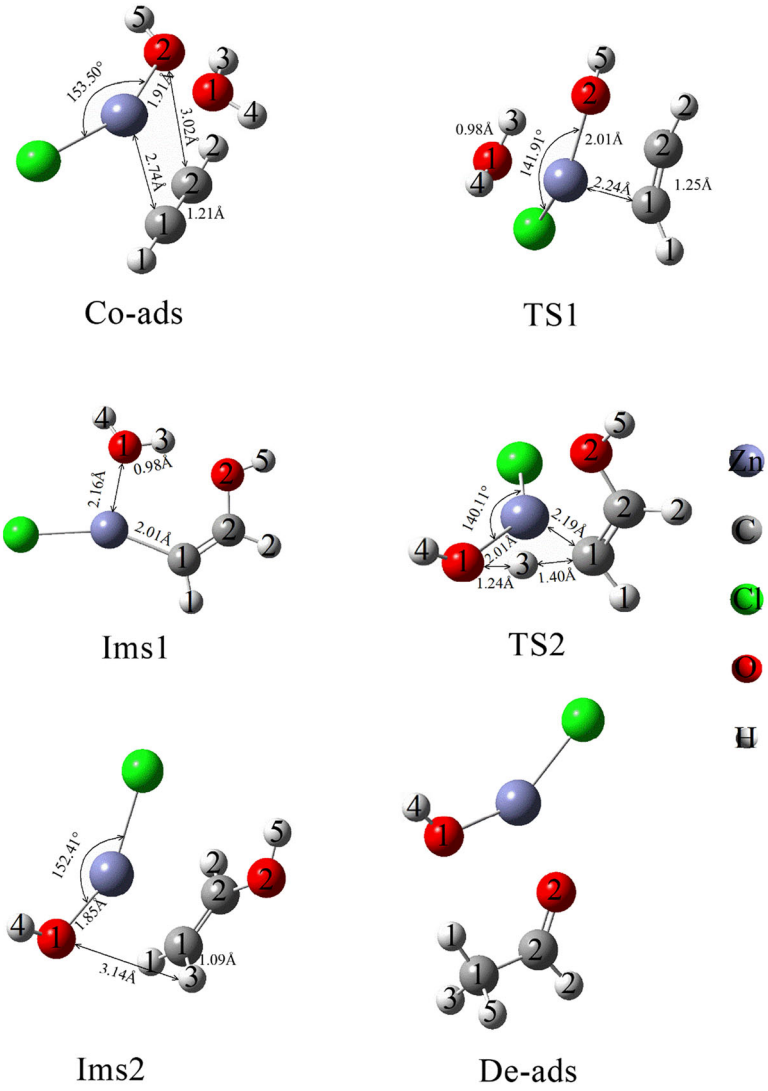

Fig. 7 Optimized structures of stationary points for the first reaction channel Zn(OH)Cl

10.90 kcal mol^{-1} was initially overcome, and the co-adsorption structure was transformed into the intermediate state (Ims1) via transition state, Ts1. The IRC calculation of this transition state confirmed that Ts1 connects the co-adsorption intermediate to Ims1, suggesting that no additional intermediates were involved in the first reaction step. Ims1 was shown to lead to Ims2 via Ts2. The pathway to Ts2 was calculated to involve participation of an H_2O molecule. The only imaginary frequency (− 1318.75 cm^{-1}) was obtained from the vibrational analysis of the Ts2 structure. To access Ts2, Ims1 indicated an energy barrier of 20.73 kcal/mol. IRC calculations were performed again to confirm that Ts2 could convert to Ims2. The final step of this reaction was similar to the previously studied catalysts and involved the release of acetaldehyde following tautomerization of vinyl alcohol.

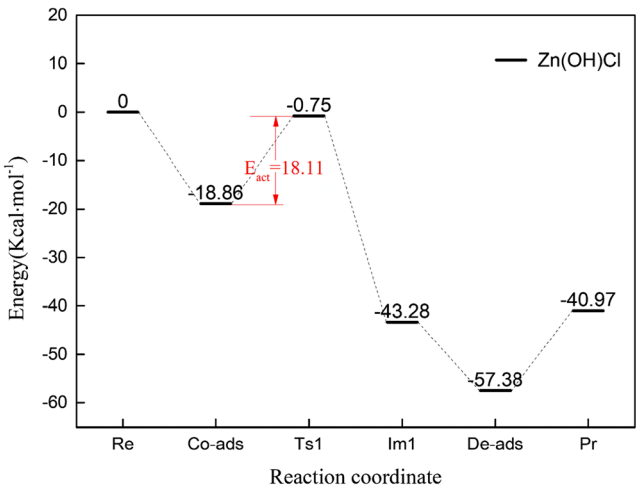

Fig. 8 The energy profiles for the second reaction pathway Zn(OH)Cl

In the second kind of reaction pathway, the reaction pathway started from the co-adsorption structure, which was converted into acetaldehyde in two steps: a distinct vinyl alcohol formation step and vinyl alcohol isomerization to form acetaldehyde. One proton from the H_2O molecule and one hydroxyl group from $Zn(OH)_2$ were

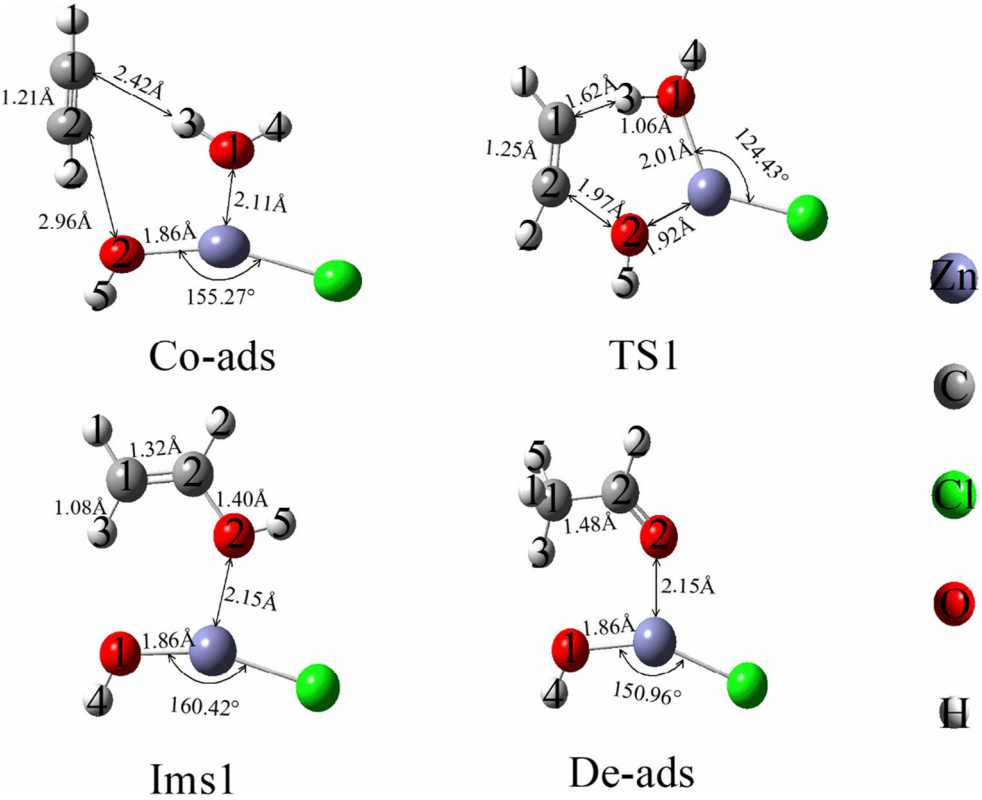

Fig. 9 Optimized structures of stationary points for the second reaction channel Zn(OH)Cl

predicted to simultaneously react with the C≡C triple bond of acetylene.

In this step, the co-adsorption structure transformed into an intermediate state (Ims1) via a transition state (Ts1). Only one imaginary frequency was found in Ts1, indicating that it is a valid transition state. The energy barrier for this step was calculated to be 19.51 kcal mol^{-1} relative to the co-adsorption state and was assigned as the rate-determining step. IRC calculations were then carried out and confirmed that Ts1 connected the co-ads state to Ims1. In Ims1, vinyl alcohol was formed, and the $Zn(OH)_2$ catalyst was regenerated. The final step of this reaction was similar to the previously studied catalysts and involved the release of acetaldehyde following tautomerization of vinyl alcohol.

Conclusions

In the present work, the hydration of acetylene to acetaldehyde catalyzed by a series of Zn catalysts ($ZnCl_2$, Zn(OH)Cl, and $Zn(OH)_2$) was theoretically studied using DFT methods. The Fukui function, condensed Fukui function, Hirshfeld charges, and ESP of the reaction processes enabled the prediction of the catalytic active sites and electron transfer information. The real acetylene hydration reaction was gas and solid phases process, we neglected the limitations of their gas-phase calculations. Some research confirmed the validity of the negligible effect of solvents on the Fukui function. We calculated different reaction pathways for the three Zn-based catalysts, providing insights into their distinct reaction mechanisms and catalytic performances.

To summarize, the catalytic performance of $ZnCl_2$ was inferior to Zn(OH)Cl and $Zn(OH)_2$. Our calculations predict that in all catalytic systems, when H_2O was added to acetylene, a vinyl alcohol intermediate was formed. Subsequently, isomerization of the alcohol afforded acetaldehyde as the desirable product. For the first kind of reaction pathway catalyzed by Zn(OH)Cl and $Zn(OH)_2$, acetylene reacted with the catalyst via interaction of its carbon atom with Zn to form a vinyl–metal complex. Meanwhile, the proton of the H_2O molecule reacted with the complex via electrophilic addition. Then, vinyl alcohol was formed, and the Zn(OH)Cl or $Zn(OH)_2$ catalyst was regenerated. Finally, tautomerization of the vinyl alcohol yielded acetaldehyde. For the second kind of reaction pathway catalyzed by Zn(OH)Cl and $Zn(OH)_2$, our calculations suggested that it undergoes a concerted mechanism. The hydroxyl group from the Zn(OH)Cl or $Zn(OH)_2$ catalyst and the hydrogen in the H_2O molecule reacted with acetylene at the same time, forming the vinyl alcohol. The isomerization of vinyl alcohol to acetaldehyde occurred in the last step.

The IRC calculations were consistent with the proposed transformations. The activation barrier for the reaction of acetylene hydration was 42.78, 21.14 (18.11), and 23.22 (19.51) kcal mol^{-1} for $ZnCl_2$, Zn(OH)Cl, and $Zn(OH)_2$,

respectively. In these three reactions, we found that the O–H bond in H_2O was relatively easy to break, lowering the activation barrier of the reaction. We anticipate that this reactivity could be exploited when designing a new acetylene hydration catalyst. We predict that Zn single atomic photocatalytic hydrolysis catalyst may be a promising catalyst applied to this reaction. Taken together, our calculations reveal that Zn(OH)Cl and $Zn(OH)_2$ are promising as catalysts for the hydration of acetylene.

References

1. Gladisch H (1969). Chem Ing Tech 41:204
2. Sobenina LN, Tomilin DN, Petrova OV, Mikhaleva AI, Trofimov BA (2013). Russ J Org Chem 49:356
3. Strauss G (1974). Chem Ing Tech. 46:132
4. Watts P, Wiles C (2007). Chem Commun:443
5. Yao S, Nakayama A, Suzuki E (2001). Catal Today 71:219
6. Schröder V, Holtappels K (2009). Chem Ing Tech 81:177
7. Trotus IT, Zimmermann T, Schuth F (2014). Chem Rev 114:1761
8. Wu X, He P, Wang X, Dai B (2017). Chem Eng J 309:172
9. Caro C, Thirunavukkarasu K, Anilkumar M, Shiju NR, Rothenberg G (2012). Adv Synth Catal 354:1327
10. Guo-rong D, Xian-zhong Y, Jin C, Bao-zhu S, Ying-jie F (2017) Huaxue Gongye (Beijing, China) 35:47
11. Idriss D, Hindermann PJ, Kiennemann B (1995). J Catal 155:219
12. Liu P, Hensen EJ (2013). J Am Chem Soc 135:14032
13. Takei T, Iguchi N, Haruta M (2011). Catal Surv Jpn 15:80
14. Hintermann L, Labonne A (2007). Synthesis:2007
15. Wu X-F, Bezier D, Darce C (2009). Adv Synth Catal 351:367
16. Budde WL, Dessy RE (1963). J Am Chem Soc 85:3964
17. Kutscheroff M, Bunsenges B (1881). Phys Chem 1540
18. Kallo D, Onyestyak G (1987) Deactivation and stabilization of late transition metal zeolite catalysts for acetylene hydration. In: Delmon B, Froment GF (eds) Studies in Surface Science and Catalysis. Elsevier, Antwerp, p 605
19. Lazo ND, White JL, Munson EJ, Lambregts M, Haw JF (1990). J Am Chem Soc 112:4050
20. Nun P, Ramón RS, Gaillard S, Nolan SP (2011). J Organomet Chem 696:7
21. Yamase T, Kurozumi T (1984). Inorg Chim Acta 83:L25
22. Yang L, Chen H, Su R, Xu C, Dai B (2018). Catal Lett 148:3370
23. Chen Z-W, Ye D-N, Qian Y-P, Ye M, Liu L-X (2013). Tetrahedron 69:6116
24. Wang Q, Zhu M, Dai B, Zhang J (2019). Cat Sci Technol 9:981
25. Wang Q, Zhu M, Zhang H, Xu C, Dai B, Zhang J (2019). Catal Commun 120:33
26. Wang Q, Zhu M, Zhang H, Xu C, Dai B, Zhang J (2018). ChemistrySelect 3:9603
27. Arita AJ, Cantada J, Grotjahn DB, Cooksy AL (2013). Organometallics 32:6867
28. Najafian A, Cundari TR (2018). Polyhedron 154:114
29. Frisch MJ, Trucks GW, Schlegel HB, Scuseria GE, Robb MA, Cheeseman JR, Scalmani G, Barone V, Mennucci B, Petersson GA, Nakatsuji H, Caricato M, Li H, Izmaylov A, Bloino J, Zheng G, Sonnenberg JL, Hada M, Ehara M, Toyota K, Fukuda R, Hasegawa J, Ishida M, Nakajima T, Honda Y, Kitao O, Nakai H, Vreven T, Montgomery Jr JA, Peralta JE, Ogliaro F, Bearpark M, Heyd JJ, Brothers E, Kudin KN, Staroverov VN, Keith T, Kobayashi R, Normand J, Raghavachari K, Rendell A, Burant JC, Iyengar SS, Tomasi J, Cossi M, Rega N, Millam JM, Klene M, Knox JE, Cross JB, Bakken V, Adamo C, Jaramillo J, Gomperts R, Stratmann RE, Yazyev O, Austin AJ, Cammi R, Pomelli C, Ochterski JW, Martin RL, Morokuma K, Zakrzewski VG, Voth GA, Salvador P, Dannenberg JJ, Dapprich S, Daniels AD, Farkas O, Foresman JB, Ortiz JV, Cioslowski J, Fox DJ (2010) Gaussian 09. Gaussian Inc, Wallingford
30. Andersson MP, Uvdal P (2005). J Phys Chem A 109:2937
31. Becke AD (1992). J Chem Phys 96:2155
32. Becke AD (1992). J Chem Phys 97:9173
33. Becke AD (1993). J Chem Phys 98:5648
34. Lee C, Yang W, Parr RG (1988). Phys Rev B 37:785
35. Boys SF, Bernardi F (1970). Mol Phys 19:553
36. Fukui K (1981). Acc Chem Res 14:363
37. Fukui K (1970). J Chem Phys 74:4161
38. Gonzalez C, Schlegel HB (1989). J Chem Phys 90:2154
39. Gonzalez C, Schlegel HB (1990). J Phys Chem 94:5523
40. Parr RG, Yang W (1984). J Am Chem Soc 106:4049
41. Yang W, Mortier WJ (1986). J Am Chem Soc 108:5708
42. Hirshfeld FL (1977). Theor Chim Acta 44:129
43. Lu T, Chen F (2012). J Comput Chem 33:580
44. Fuentealba P, Pérez P, Contreras R (2000). J Chem Phys 113:2544
45. Ola'h J, Van Alsenoy C, Sannigrahi AB (2002). J Phys Chem A 106:3885